Hindawi
International Journal of Aerospace Engineering
Volume 2018, Article ID 2894908, 14 pages
https://doi.org/10.1155/2018/2894908

Research Article

Experimental Study of Spray Characteristics of Kerosene-Ethanol Blends from a Pressure-Swirl Nozzle

Tao Zhang, Bo Dong, Xun Zhou, Linan Guan, Weizhong Li, and Shengqi Zhou

Key Laboratory of Ocean Energy Utilization and Energy Conservation of Ministry of Education, Dalian University of Technology, Dalian 116024, China

Correspondence should be addressed to Weizhong Li; wzhongli@dlut.edu.cn

Received 1 March 2018; Revised 3 July 2018; Accepted 5 September 2018; Published 7 November 2018

Academic Editor: André Cavalieri

Partial replacement of kerosene by ethanol in a gas turbine is regarded as a good way to improve the spray quality and reduce the fossil energy consumption. The present work is aimed at studying the spray characteristics of kerosene-ethanol blends discharging from a pressure-swirl nozzle. The spray cone angle, discharge coefficient, breakup length, and velocity distribution are obtained by particle image velocimetry, while droplet size is acquired by particle/droplet imaging analysis. Kerosene, E10 (10% ethanol, 90% kerosene), E20 (20% ethanol, 80% kerosene), and E30 (30% ethanol, 70% kerosene) have been considered under the injection pressure of 0.1–1 MPa. The results show that as injection pressure is increased, the discharge coefficient and breakup length decrease, while the spray cone angle, drop size, and spray velocity increase. Meanwhile, the drop size decreases and the spray velocity increases with ethanol concentration when the injection pressure is lower than 0.8 MPa. However, the spray characteristics are not affected obviously by the ethanol concentration when the injection pressure exceeds 0.8 MPa. A relation to breakup length for kerosene-ethanol blends is obtained. The findings demonstrate that the adding of ethanol into kerosene can promote atomization performance.

1. Introduction

With the rapid emergence of serious energy consumption, there have been growing concerns about exhaust emissions, particularly about emissions of CO, HC, and particulate matter. A gas turbine is generally considered as the "heart" of an aviation aircraft or a power plant. The burning of fossil fuels in these devices consequently causes energy-related and environmental problems. Especially in the aviation and aerospace industries, a series of complex chemical and physical changes in combustion processes occur, and pollutants are inevitably produced. It has been pointed out that the interactions of various emitted pollutants are significantly affected by fuel properties such as fuel density, viscosity, and surface tension [1–5].

In order to improve the atomizing quality and reduce the pollutant emissions, engineers devote themselves to changing the fuel properties by using conventional fuels blended with renewable fuels such as biodiesel [6], alcohols [7–9], and Jatropha oils [10]. For example, in Brazil and the United States [11, 12], alcohol, a renewable resource, was blended with gasoline or diesel in different proportions, and then the mixture was used in the aviation sector. Consequently, there are studies focusing on engine-related fuels including gasoline-ethanol, diesel-ethanol, and jet-A fuel-ethanol mixtures along with the comparison of operational thrust and emissions of pollutants resulting from these fuels. Bayraktar [13] used the gasoline-ethanol blends in engines, which dramatically reduce the pollutant emissions. The study showed that the blend of 7.5% ethanol is the optimum mixing volume ratio for the fuel mixture. However, in theoretical analysis, 16.5% ethanol is found to be the optimum value. Overall, the adding of ethanol into gasoline could improve the fuel combustion. In addition, ethanol is a renewable energy source, and it has been considered as the well-suited fuel for spark-ignition engines. So utilization of ethanol as additive fuel has a promising future in gas combustion engines. Meanwhile, ethanol has broad flammability limits,

high octane numbers, flame speeds, and latent heats of vaporization [14]; it is desired to study the spray characteristics of kerosene-ethanol.

Generally, the spray quality is mainly characterized by the spray cone angle, discharge coefficient, and breakup length. Firstly, the spray cone angle and spray velocity of the pressure-swirl nozzle affect the fuel combustion and emission of the pollutants. Reduction in the spray cone angle is benificial for the increase in combustion efficiency at low power conditions. However, a larger spray cone angle and a higher spray velocity lead to better gas-fuel mixing and wider fuel coverage area. Moreover, it has been pointed out that they are influenced by liquid properties [15]. More dispersion results in lower fuel concentrations, which leads to lower emissions and less soot formation. So, the spray cone angle is a main factor affecting the spray characteristics, and it determines the success of the ignition [16]. Secondly, the discharge coefficient specifies the utilization efficiency of energy. A low discharge coefficient shows that there are a few liquid momentum losses in the nozzle chamber [17]. In addition, the breakup length is a key factor for the liner size design, since a decrease in the breakup length can reduce the length of the flame tube [18]. Lee et al. [19] found that breakup length decreases with injection pressure. A short liquid breakup length means that liquid sheets break into ligaments and then drop quickly. Meanwhile, the above-mentioned factors not only affect each other but also are the dominant roles for steady output power and quiet combustion. So far, there are plenty of literatures about spray characteristics of kerosene. However, little attention has been paid to the spray quality of kerosene-ethanol blends. Recently, Song et al. [20] experimentally studied the spray characteristics of ethanol-kerosene blended fuels. They found that the addition of ethanol has a certain effect on the spray characteristics. Yet, the results denoted that the blend of 20% ethanol in kerosene does not significantly affect spray performance compared with kerosene. Their study focused on the spray characteristics of the direct jet nozzle only; consequently, the conclusion is not suitable for the pressure-swirl nozzle.

In the present work, the spray characteristics of kerosene and ethanol blends discharging from a pressure-swirl nozzle are experimentally studied in the spray chamber under ambient temperature and pressure conditions. Ethanol is added with the ratios of 10%, 20%, and 30% by volume into kerosene. The spray cone angle, discharge coefficient, breakup length, spray droplet velocity, and droplet size are examined in detail.

2. Experiment

2.1. Pressure-Swirl Nozzle. A single-hole pressure-swirl nozzle is used in the present study. The critical geometrical dimensions of the nozzle and route of fluid flow are shown in Figure 1. The injector produces a hollow-cone spray. The discharge orifice diameter d_0 is 0.8 mm, the orifice length l_0 is 1.5 mm, the diameter of swirl slot d_i is 0.2 mm, the swirler angle (β) is 30°, and the length l_s and diameter D_s of the swirl chamber are 5.2 and 5 mm, respectively. The fuel

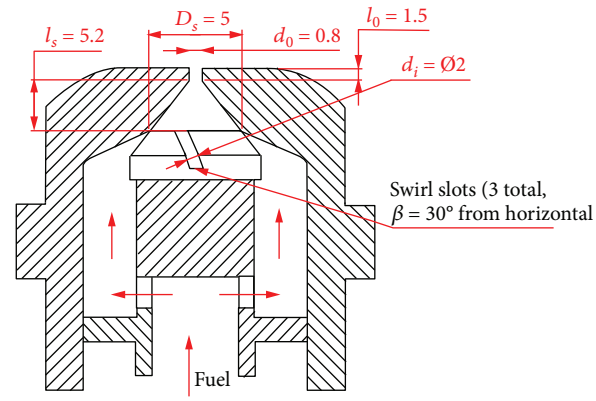

Figure 1: Schematic of a pressure-swirl nozzle. (All dimensions are in millimeters.)

is pressured into the swirl chamber through three slots with high angular velocity. There exists a swirl flow of the liquid in the swirl chamber. The fuel is discharged through this nozzle exit in the form of a hollow-cone formation under centrifugal force. As the liquid film develops, it becomes an instability wave and then disintegrates into small droplets.

2.2. Experimental Setup. The experimental setup of the particle image velocimetry (PIV) system is shown in Figure 2. The spray characteristic testing system consists of a set of optical devices, a spray chamber, a fuel transport and return system, and some other auxiliary equipment. The blended fuel is stirred to achieve uniformity, and then it is injected into the nozzle by means of a gear pump. The pressure or mass flow rate can be controlled by the rotating speed of the motor in the gear pump. The injection pressure is recorded by a piezometer mounted on the nozzle. Pressure sensors with an accuracy of ±0.5% are used to monitor the pressure of the liquid system. The mass flow rate of the fuel is measured by a liquid flowmeter, with a measuring range of 2.1–139.2 L/h and an accuracy of ±0.2%. The blended fuel is charged into the spray chamber. There is a buffer fuel tank installed between the gear pump and the nozzle. The pulse in the fuel tube can be removed by the buffer fuel tank. The nozzle is mounted downwardly on a vertical plane. The spray is shone by the laser sheet, and it can be observed through the quartz glass by a camera. The fuel and signal line diagram of the test rig is also clearly shown in Figure 2.

The spray cone angle and spray velocity field are measured by the PIV. Illumination is provided by the dual-cavity neodymium-doped yttrium aluminium garnet (Nd:YAG) laser, with 50 mJ pulse, 8 ns duration, 10 Hz frequency, and 532 nm wavelength, in conjunction with a light sheet to shine the spray. The laser sheet is adjusted to nearly 1 mm. The pictures are snapshot by a CCD camera with the following specifications: 1376×1040 resolution, 12-bit digital image, and a magnification of 3.2. The camera response is guaranteed consistent with the laser sheet by the programmable timing unit (PTU).

The PIV can capture two frames that straddle the two pulsed lasers through the sheet optics. The raw images recorded by the CCD are transferred to a computer. Some

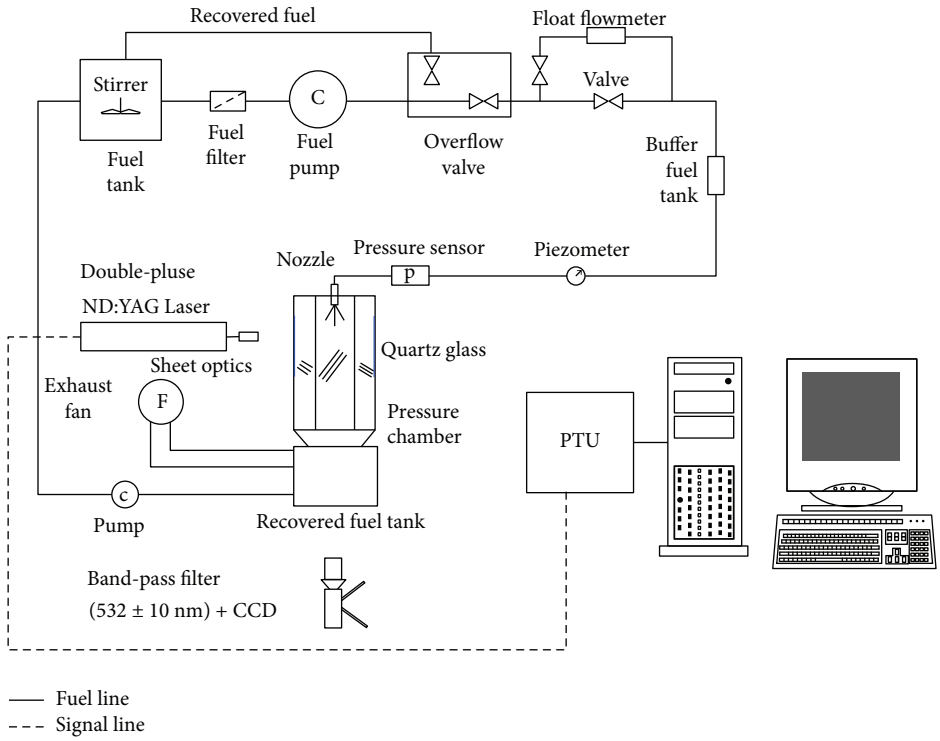

Figure 2: Schematics of the PIV system.

status data relating to the particle velocimetry are then analyzed and displayed by the DaVis 8.1 software from LaVision Company. The synchronized working time between the CCD camera and the double-pulsed laser is provided by the PTU.

The field of view (FOV) of spray velocity is 40×51 mm. The particle velocity range is restricted in an appropriate range, which depends on the injection pressure. The velocities are estimated by a correlation process based on multigrid interrogation (decreasing size). The initial and final window sizes are selected to be 64×64, 48×48 pixels, respectively. The smaller interrogation window size leads to less spurious vectors. This way utilizes the vector results acquired by processing the initial interrogation region for predicting the results concerning the next interrogation area. A relative overlap of 25% among adjacent interrogation areas is applied for compensating the absence of the vector field during the velocity post-processing. Vectors in the interrogation region where the peak ratio is higher than 1.3 are validated. Individual vectors are compared to the local vectors in a neighborhood vector area (5×5 pixel size). More iterations can smooth the spray velocity, but it is time-consuming. The detected spurious vectors are cut off and replaced by local interpolated vectors using 5 iterations. Spurious vectors are identified via an acceptance factor of 15% on velocity vector gradient in the region. If the calculated gradient is larger than the set value, the central vector will be cut off. During the post-processing, in order to keep the completeness of velocity distribution, a little empty space could be filled up through interpolation, which almost has no influence on the actual velocity field.

Figure 3 shows the experimental setup for spray visualization and droplet sizing. The imaging technique used in this study is the shadowgraph for the spray structure, and the lens is attached to the camera [21]. Most part of the shadowgraph setup is the same as the PIV system except for the optical imaging system. So only the details of the optical experimental facility are depicted in Figure 3. A dual-cavity Nd:YAG laser is used as the illumination backlight to freeze the shot-to-shot atomization process. The disintegration of liquid sheet can be obtained from this system. These images can be used to obtain the liquid breakup length.

In the particle/droplet imaging analysis (PDIA), the lens of the camera is replaced by a long-distance microscope (LDM) for droplet sizing. In order to measure droplet size, a much smaller region of the spray (3.4×3.2 mm) is photographed using a long-distance microscope. The PDIA, based on high-resolution imaging with pulsed backlight illumination, is used to visualize spray droplets. The measurement volume is defined by the focal plane and the depth of field of this system. This technique is independent of the shape and material (either transparent or opaque) of the particles, and it allows investigation of sizes down to $5\,\mu$m using an appropriate imaging system and light source.

2.3. Fuel Properties. The fuels used in this experiment are Chinese standard commercial kerosene and ethanol. Four fuels adopted are 100% kerosene and mixtures of kerosene and ethanol containing 10%, 20%, and 30% ethanol by volume, which are labelled as E10, E20, and E30, respectively (the number represents the percentage of ethanol). The density, kinematic viscosity, and surface tension of blends are tested by the densimeter, viscometer, and surface tension meter, respectively. Table 1 shows the blended fuel

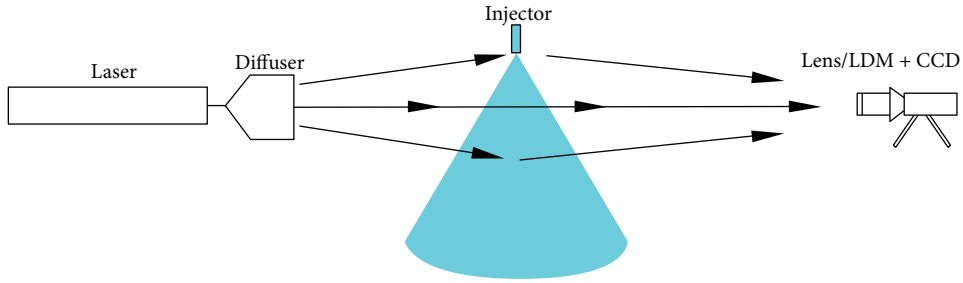

Figure 3: Experimental setup for spray visualization and droplet sizing.

Table 1: Fuel properties.

Liquid (volume fraction)	Kinematic viscosity (μ_l, mm^2/s)	Density (ρ_l, kg/m^3)
Kerosene	2.30	802.0
Kerosene (90%)-ethanol (10%) (E10)	2.18	801.1
Kerosene (80%)-ethanol (20%) (E20)	2.03	799.2
Kerosene (70%)-ethanol (30%) (E30)	1.89	798.1
Ethanol	0.90	789.0

properties. The surface tension and density of the kerosene and ethanol are almost the same.

3. Results and Discussion

In this section, a group of 50 successive paired images are captured with the injection pressure in 0.1 MPa–1.0 MPa. The spray cone angle, discharge coefficient, breakup length, spray velocity, and droplet size are discussed as follows.

3.1. Spray Cone Angle. The spray cone angle, defined as the largest angle formed by the two straight lines from the nozzle tip to the boundary of the spray [22], is an important factor determining the liquid dispersion of the kerosene-ethanol blends. For a gas engine, an optimum cone angle yields a short penetration and small droplets. In the experiments, the spray cone angles are obtained in a steady spray state and controlled by changing the injection pressure and ethanol concentration in the fuel blends. Figure 4 presents the relationship between the spray cone angle and the injection pressure. The results indicate that when the injection pressure is less than 0.8 MPa, the spray cone angle increases with the injection pressure, which is in agreement with the experimental works of Rashid et al. [23] and numerical findings of Datta and Som [24]. When the injection pressure is beyond 0.8 MPa, the spray cone angles of all blends attain the maximum value (nearly 80°), which is the design value of the nozzle.

At any injection pressure, the spray cone angle becomes large as the ethanol concentration increases. Compared with kerosene, the spray cone angles of E10, E20, and E30 increase on average by 2.58%, 5.15%, and 7.87%, respectively. The

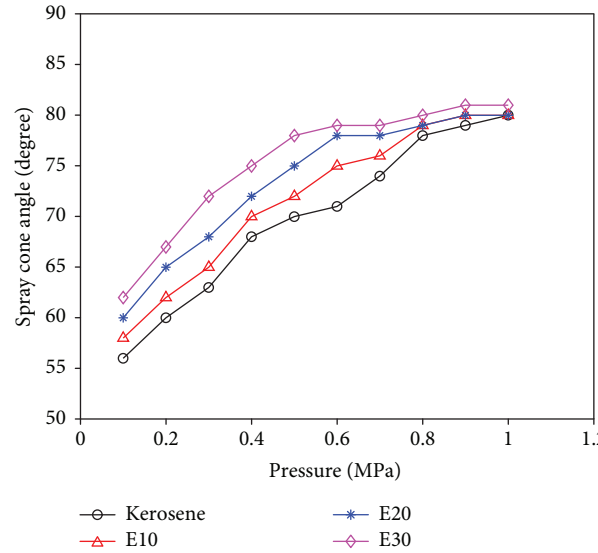

Figure 4: Variation of spray cone angles of kerosene and the blends with the injection pressure.

effect of ethanol addition on the spray cone angle becomes more distinct at lower pressure. For fuels with high ethanol concentration, the viscosity is small. Thus, the spray cone angle increases as viscosity decreases, which is in agreement with the results described in previous studies [25, 26]. This can be attributed to the fact that the azimuthal velocity inside the swirl chamber is due to high viscosity.

Generally, considering the effects of viscosity and injection pressure, the empirical formula of the spray cone angle for a pressure-swirl nozzle for kerosene was proposed by Lefebvre [22] as

$$2\theta = 6K^{-0.15}\left(\frac{Pd_0^{\,2}\rho_l}{\mu_l^{\,2}}\right), \quad (1)$$

where θ is the spray cone angle, K is the nozzle constant, and P is the injection pressure. Here, (1) is applied to predict the spray cone angle for the blended fuels. Figure 5 shows the comparison of the spray cone angle between the predicted values and the experimental results. It can be found out that the maximum relative errors are less than (±9%), so it can be proved that the empirical formula by Lefebvre is also suitable for kerosene-ethanol blends.

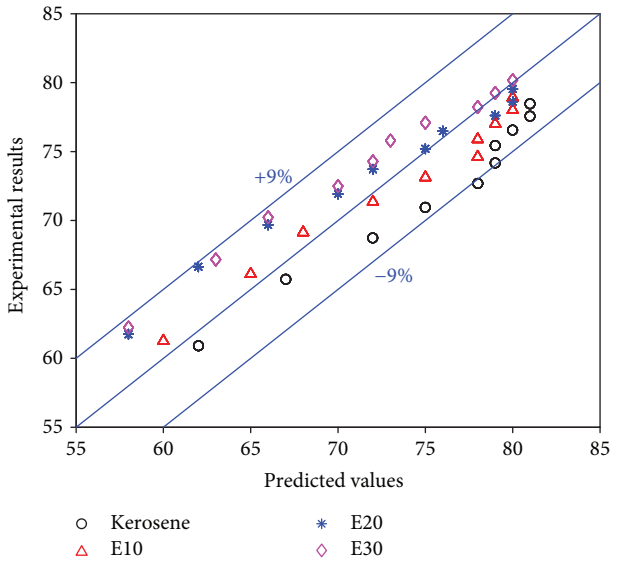

Figure 5: Scatter of measurement data points of spray cone angle with respect to (1).

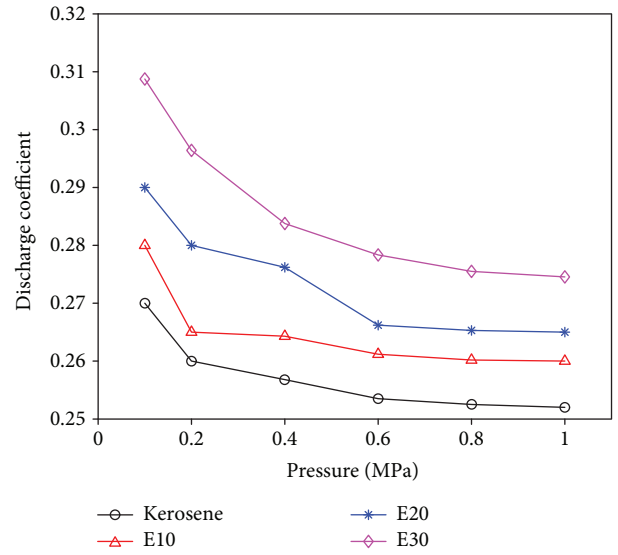

Figure 6: Variation of the discharge coefficient of the pressure-swirl nozzle with injection pressure.

3.2. Discharge Coefficient. In the current study, the volumetric flow rate Q is measured by the mass flowmeter installed at the inlet of the nozzle, and the fuel exit velocity v is calculated by

$$v = \frac{Q}{A}, \tag{2}$$

where A is the cross-sectional area of the nozzle orifice. The nozzle discharge coefficient C_d is defined as

$$C_d = \frac{v}{\sqrt{2P/\rho_l}}. \tag{3}$$

The discharge coefficient specifies the pressure loss across the nozzle as it represents the ratio of the actual flow rate to the theoretical flow rate. The values of the discharge coefficient for blended fuels are plotted as a function of the injection pressure, and the results for the four fuels are shown in Figure 6. It can be seen that the discharge coefficient decreases with the injection pressure and finally approached to a relatively stable value. This is consistent with the results obtained by Lan et al. [27] and Soltani et al. [28]. Moreover, the discharge coefficient of the pressure-swirl nozzle is inevitably small. This is due to the emerging of the air core, which directly blocks off the center of the swirl chamber. Once in the low injection pressure regime, the discharge coefficient becomes insensitive to the injection pressure. The mass flow rate reaches its maximum value (design value), and no further increase in the radial spray velocity is achievable. So the discharge coefficient becomes steady under high-pressure conditions. Compared with kerosene, the discharge coefficients of E10, E20, and E30 decrease on average by 4.3%, 7.4%, and 10.1%, respectively. The variation of the discharge coefficient with ethanol concentration can be attributed to the viscosity as well. For low ethanol concentrations (high viscosity), the viscous force prevents the fuel discharging from the nozzle, and there is more friction loss in the nozzle. Higher liquid viscosity leads to less swirl strength, which results in lower velocity outside of the nozzle.

As for the pressure-swirl nozzles, Jones obtained the following empirical equation for the discharge coefficient as [22]

$$C_d = 0.45\left(\frac{d_0\rho_l v}{\mu_l}\right)^{-0.02}\left(\frac{l_0}{d_0}\right)^{-0.03}\left(\frac{l_s}{D_s}\right)^{-0.05}\left(\frac{A_i}{d_0 D_s}\right)^{0.52}\left(\frac{D_s}{d_0}\right)^{0.23}, \tag{4}$$

where A_i is the total inlet slot sectional area. The size of the nozzle is considered as quantitative; then, (4) can be rewritten as

$$C_d = 0.3752\left(\frac{\rho_l v}{u_l}\right)^{-0.02}. \tag{5}$$

The comparison between predicted values of the discharge coefficient by (5) and experimental data is given in Figure 7. It can be found out that the predicted values are generally larger than the experimental results, because (5) is derived for the pressure-swirl nozzle with swirler angle $\beta = 0$. The bigger swirl angle leads to a smaller discharge coefficient [29]. However, the pressure-swirl nozzle with $\beta = 30^\circ$ is investigated in the current study. The maximum relative error and average error are 14.2% and 6.8%, respectively.

3.3. Breakup Length. The breakup length is measured from the nozzle orifice to the region of drop formation where the film breaks up into ligament or droplets [30]. Figure 8 shows the schematic of liquid breakup length for the pressure-swirl

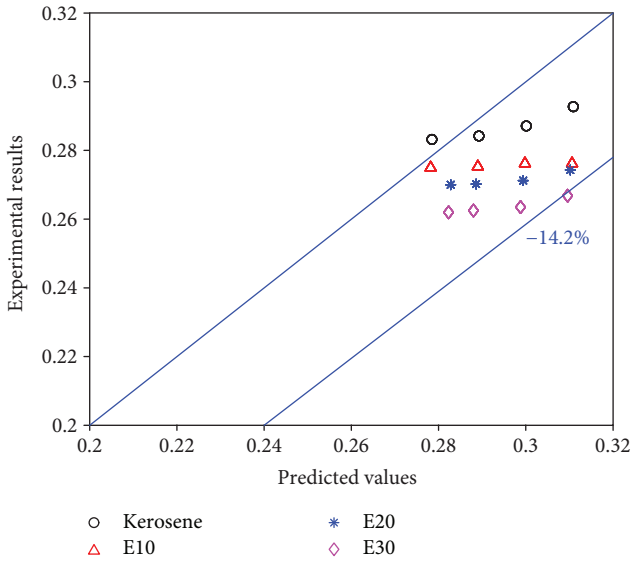

Figure 7: Scatter of measurement data points of C_d with respect to (5).

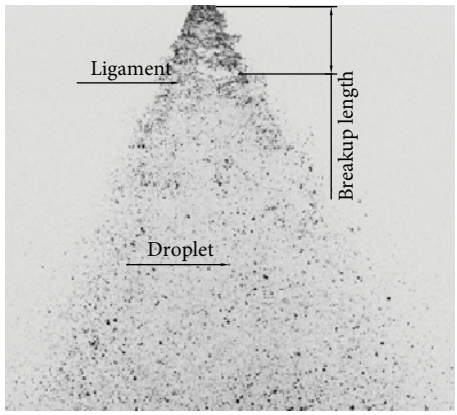

Figure 8: Breakup length of swirl liquid from pressure-swirl nozzle.

nozzle. Though the region of fuel sheet breakup is very clear, the precise point or location where the liquid breaks up into droplets is hard to obtain. In other words, this point is the ending position of the first atomization. In this paper, a specific method is used to calculate the breakup length as follows. The spray body is divided into M pieces by the horizontal lines (L_j). The spacing between the adjacent two horizontal lines is set to 0.2 mm. The light intensity (I_j) on the horizontal line is obtained and averaged by Matlab software. Every horizontal line is then divided into N equal parts with the spacing of 0.1 mm. In the spray body, the segmentation amount varies with the horizontal lines. The light intensity ($I_{(i,j)}$) of every node can be obtained by Matlab software. The schematic diagram of light intensity is shown in Figure 9. A relationship between the averaged value of light intensity on the horizontal line $I_y = (1/n)\sum_{i=1}^{n} I(x_i, y_j)$ and the spray axis (y) is described in Figure 10. The liquid is shone by the laser light as a light source, and it is colorized to emphasize the intensity range (0–2000 counts). The liquid film in the spray has a high brightness level than those of liquid droplets in the spray. The droplets with the low brightness in the spray mean that the number of droplets or liquid film is decreased by fine atomization and quick evaporation. So, there is an obvious difference in light intensity between the liquid and droplets. When the liquid has been already disintegrated into droplets, the light intensity of liquid will not change in a wide range. In Figure 10, the light intensity below the marked point A only fluctuates within a narrow range along the y-axis, so the marked point A is the end point of liquid film breaking into droplets. Consequently, it is assumed to be the precise location where the most part of liquid sheet has broken into droplets. In this condition, the breakup length is defined as the distance from the nozzle exit to the marked point A. Under every condition, 50 successive images are sampled for the breakup length and standard deviation calculation; these deviations are indicated as the error bars in the plots.

Figure 11 shows the variation of breakup length for all blends with injection pressure under steady spray conditions. The breakup length decreases with injection pressure. The pressure increase results in more kinetic energy, causing more spread of the fuel film. In the steady spray, the liquid bulb starts to open up due to the surface breakup. Almost all the kinetic energy disrupts the liquid sheets breaking into ligaments or droplets. This causes a reduction in liquid breakup length with the injection pressure. Under a certain injection pressure, the breakup length decreases with the ethanol concentration. Compared with kerosene, the breakup lengths of E10, E20, and E30 decrease on average by 10.6%, 20.3%, and 43.1%, respectively. The results show that the viscous force plays an important role in consolidating the liquid into a compact form. This phenomenon is also observed in a previous study [18]. The liquid viscosity acts to reduce the liquid wave growth. Therefore, at a given injection pressure, the liquid with a higher viscosity is more resistant to break up by the aerodynamic drag. Under these spray conditions, the low viscosity liquid tends to shorten the breakup length and promote atomization.

Han et al. [31] proposed a semiempirical relation to estimate the breakup length of the pressure-swirl nozzle

$$L = C\left(\frac{\rho_l \sigma h \ln(\eta_b/\eta_0)\cos\theta}{\rho_g^2 V^2}\right)^{0.5}, \quad (6)$$

where C is an experimental constant, and it equals 3.0 in their study for water. As for the blended fuels considered in the current study, it is modified to 6.7 based on the experimental data. The liquid film in the nozzle is calculated by $h = 3.66(Qd_0\mu/P)^{0.25}$, and the liquid sheet velocity is obtained by $V = Q/\pi(d_0 - h)h$ [32]. The ambient gas density ρ_g is 1.12 kg/m^3. The quantity $\ln(\eta_b/\eta_0)$ is given the values 12 and 2.5 suggested by Dombrowski and Hooper [33] and Han et al. [31], respectively. The amplitude of the initial surface wave η_0 and the amplitude of the disturbance wave η_b when the breakup takes place can be measured by the 50

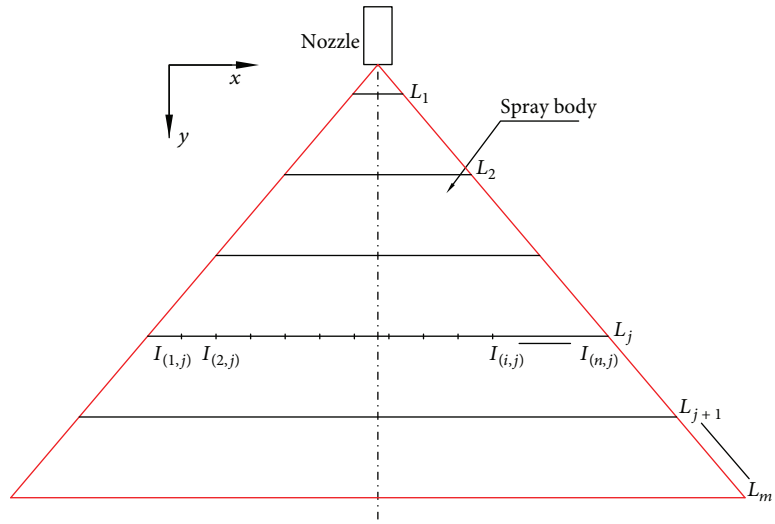

Figure 9: The diagram of local light intensity corresponding to the point in the spray body.

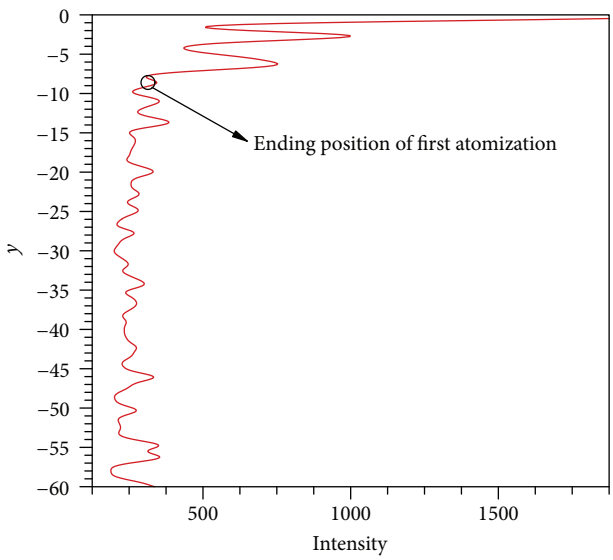

Figure 10: The average light intensity (I_y) varies along the axial distance (y).

successive images. Figure 12 shows the measured η_b and η_0 in one operating condition. Figure 12(a) is captured by shadowgraph using the lens while Figure 12(b) is snapshot by the LDM. This measured method is documented by other investigations of hollow-cone sprays from the pressure-swirl nozzle [34, 35]. The terms ln (η_b/η_0) are set to 4.2, 4.0, 4.0, and 3.0 for kerosene, E10, E20, and E30 on the basis of experimental data.

Figure 11 also shows the comparison between experimental data of breakup length with semiempirical predictions, as indicated by the dashed line. The relative errors between the experimental values of kerosene, E10, E20, and E30 and valves predicted by (6) (Han's semiempirical relation) are 1.5% (−5.0%), −8.6% (5.7%), −7.2% (19.2%), and 3.4% (67.0%), respectively. The constant C and ln (η_b/η_0) obtained by Han et al. are not appropriate for kerosene-ethanol. So, the modified formulation is more suitable for estimating the breakup length of the pressure-swirl nozzle than those predicted by Han et al.'s semiempirical relation.

3.4. PIV Droplet Velocity Analysis. Figures 13–15 show the results of the blended fuel droplet velocity distribution in the axial cross section of the spray at different injection pressures. There is high spatial variability with the maximum velocity at a very short distance below the nozzle exit. Velocity magnitude distribution in the spray shows a significant dependence on the injection pressure. Spray droplets are used as the tracer particles for the calculation of velocity vectors. PIV cannot correctly capture the velocity in areas with high droplet concentration [36]. Therefore, the velocity field near the nozzle orifice is not shown in Figures 13–15. Hollow-cone spray formation is produced at high pressure; especially, this phenomenon occurs obviously at 0.5 MPa and 0.8 MPa. The spray is divided into two main jets propagating along the spray periphery. The widening spray cone intensifies the droplet interaction with air, and the droplet momentum decreases along the downstream distance sharply, as shown in Figures 13–15. Figure 16 shows that the maximal spray velocity increases as the ethanol concentration in the profile of $y = -20$ mm.

At 0.2 MPa, the blended fuel sprays form the hollow-cone shape. Only for the kerosene condition does spray tend to become solid-cone rather than hollow-cone. The reason is that the viscosity of ethanol is lower than other fuels; the fuel with high ethanol concentration easily gets more momentum to develop the spray under the radial direction. A maximum velocity of 12 m/s is recorded for E30 while 8 m/s is arrived by the kerosene spray. The maximum velocity increases with the ethanol concentration in the blended fuel. Compared with kerosene, the maximum velocity at $y = -20$ mm of E10, E20, and E30 rise by 37.8%, 78.8%, and 111.1%, respectively. The velocity distribution area also expands with the ethanol concentration. The larger velocity corresponds to a wider spray cone angle and more dispersion. The increases in

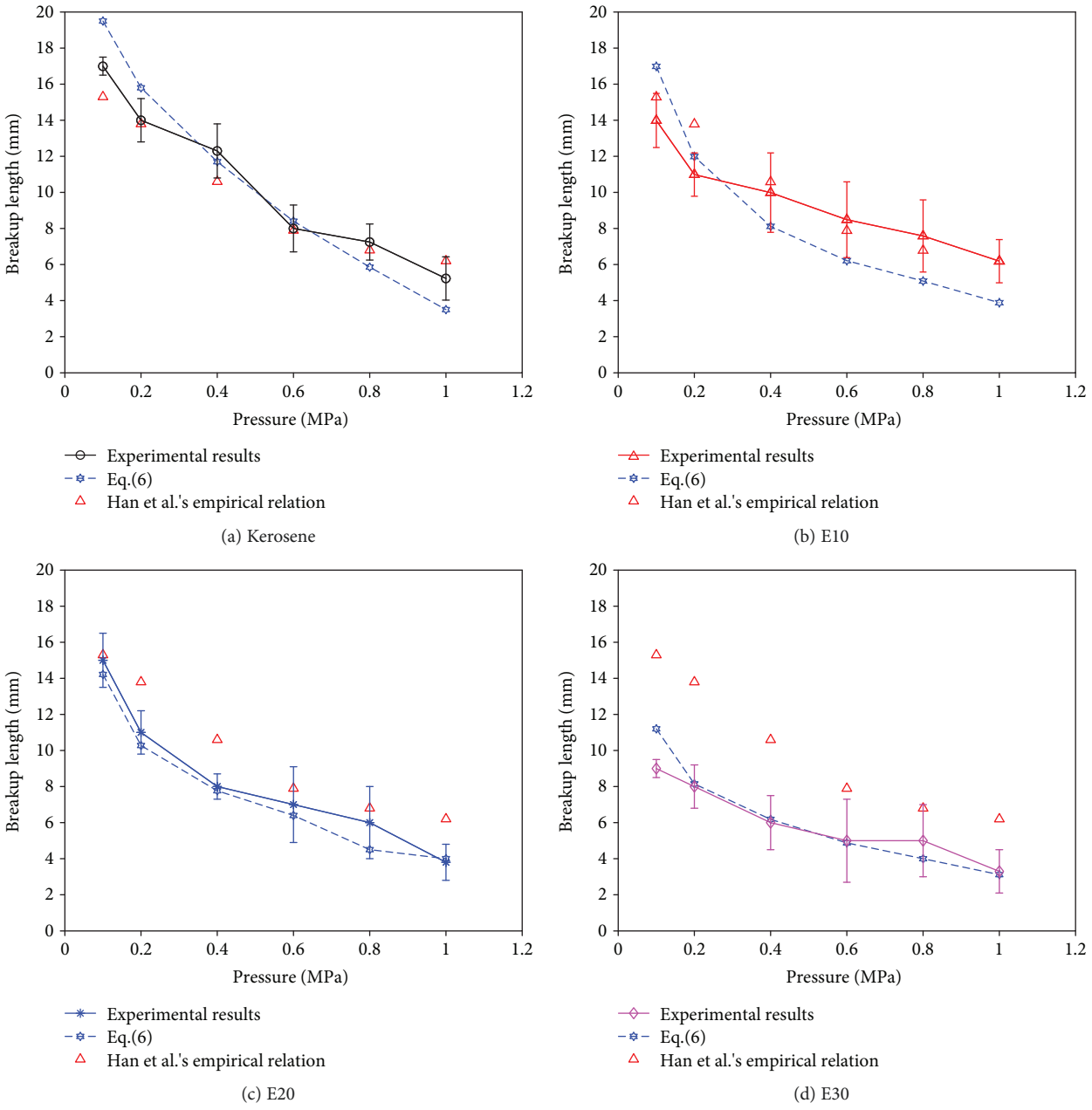

Figure 11: Variation of liquid breakup length with injection pressure.

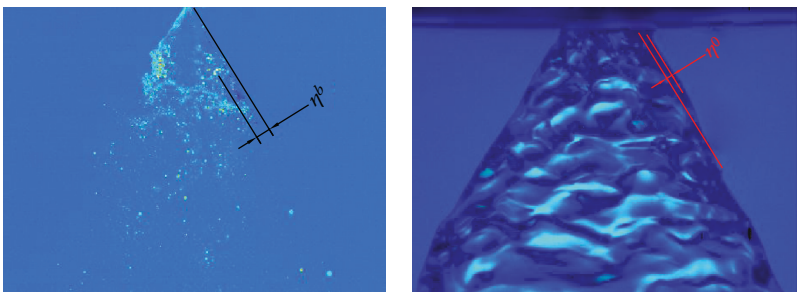

(a) Spray region (40 × 51 mm) (b) Spray region (3.4 × 3.2 mm)

Figure 12: Schematic of the amplitude of the disturbance on the liquid sheet.

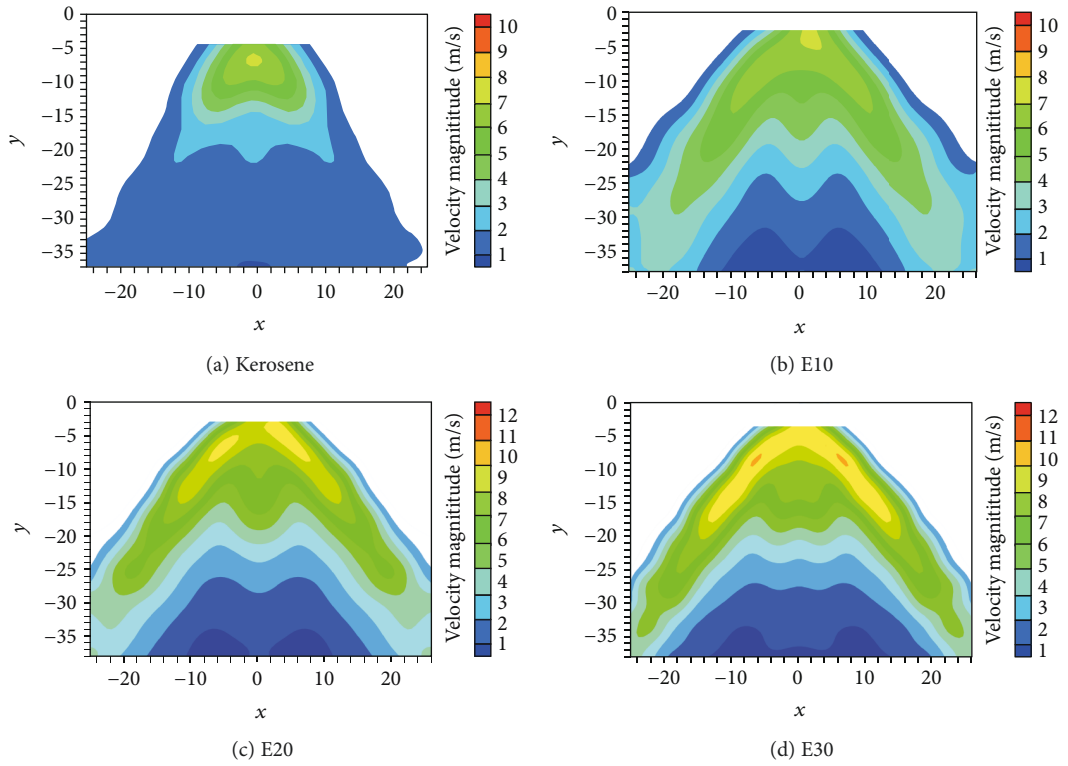

Figure 13: Velocity magnitudes at 0.2 MPa.

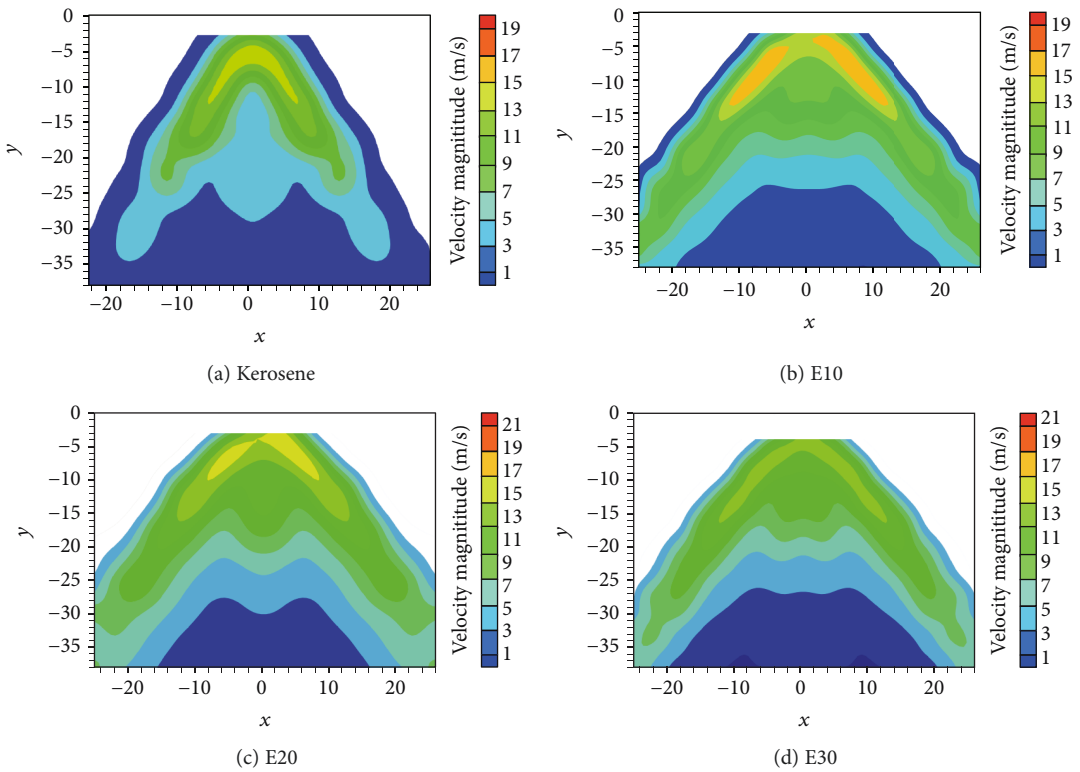

Figure 14: Velocity magnitudes at 0.5 MPa.

ethanol concentration can prompt the solid-cone changing into hollow-cone spray, which is the typical feature of the pressure-swirl nozzle. Based on the above analysis, the velocity distribution is sensitive to the ethanol concentration, which is beneficial for forming the hollow-cone spray under low pressure.

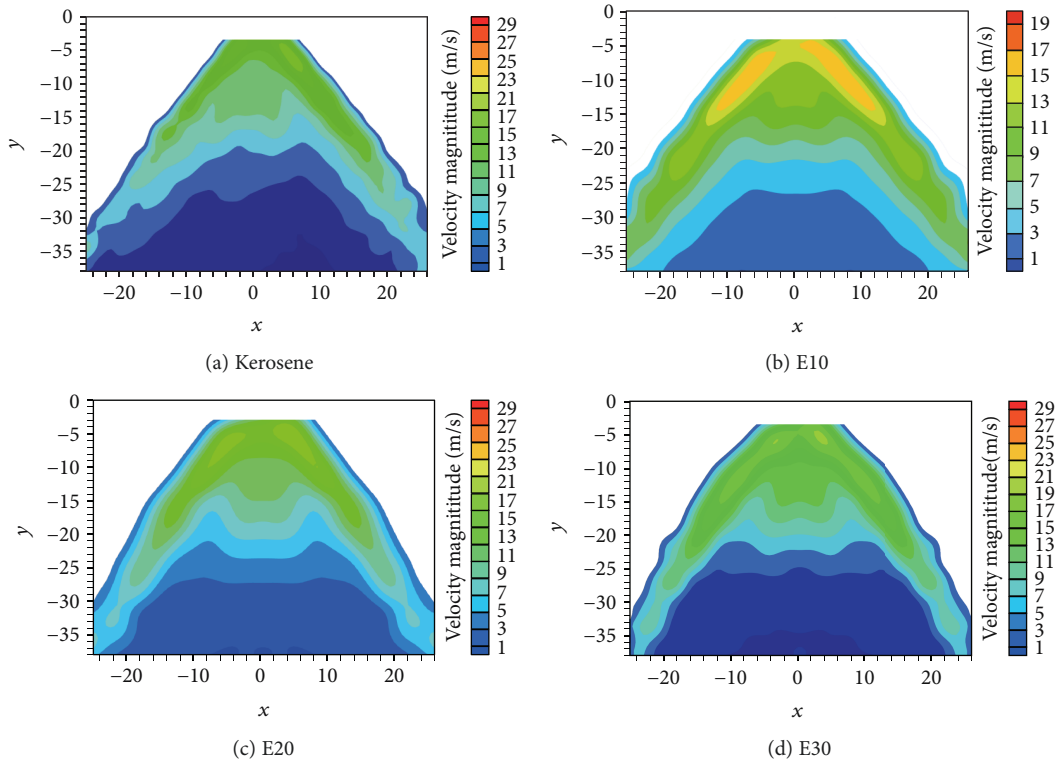

Figure 15: Blended fuel velocity magnitudes at 0.8 MPa.

At 0.5 MPa, the hollow-cone sprays are produced by this pressure-swirl nozzle. The spray velocity maxima also increase with the ethanol concentration. Compared with kerosene, the maximum velocities at $y = -20$ mm of E10, E20, and E30 rise by 9.4%, 11.8%, and 23.1%, respectively. The spray velocity of fuel with high ethanol concentration is prone to attaining high value after disintegration of the liquid sheet. From the velocity distribution, it is found that kerosene is hard to diffuse and form a hollow cone because of its high viscosity. High viscosity could prevent the pressure-swirl nozzle from sustaining a centrifugal-driven air core within the fuel nozzle. Figure 14 shows that the hollow-cone area of kerosene is obviously smaller than the other blended fuels. A strong internal swirl intensity means that the high spray velocity of the liquid droplet is produced outside the nozzle. An increase in liquid viscosity results in a liquid sheet with few waves and great resistance to breakup [3].

At 0.8 MPa, with sufficient swirl at present high pressure, the blended liquid sheets generate the hollow-cone conical spray structure. This means that the high-velocity region is almost located in the spray periphery for all fuels. The external sprays are stable, and they develop into a fully cone shape regardless of the ethanol concentration. The shapes of the hollow cone are almost the same; so is the spray cone angle. The ethanol concentration has slight influence on the spray velocity distribution characteristics. Compared with kerosene, the maximum velocities at $y = -20$ mm of E10, E20, and E30 rise by 5.4%, 6.5%, and 21.2%, respectively. The gap among the spray velocities of blended fuels becomes narrow as the injection pressure increases. Under high-pressure conditions, the distributions of the velocity profile are mainly limited by the nozzle geometry and size. As above-mentioned, at high pressure, the velocity distributions are almost the same whatever the ethanol concentration in the blended fuel.

3.5. Droplet Size Analysis. The blended fuel particle size produced by the pressure-swirl nozzle varies with injection pressure. Figure 17 shows the sample microscopic FOV of about 3.4 mm × 3.2 mm, which is located at $y = -25$ mm downstream. The droplet size of FOV is measured every 5 mm from $x = -25$ mm to 25 mm in the radial direction. All the measured points are shown in Figure 18. A set of 50 image pairs for each FOV are obtained, and the detection of the droplet diameter is performed based on an automated segmentation threshold algorithm to determine whether a droplet is in the focal plane. The sauter (or surface weighted) mean diameter (SMD) is selected to represent the mean diameter of droplets within the flotation cell, since it is particularly relevant to hydrodynamics and mass transfer.

Figure 19 shows the SMD of the blended fuels at various radial distances for 25 mm from downstream of the nozzle under different injection pressure conditions (0.1 MPa, 0.5 MPa, and 0.8 MPa). The SMD of droplets around the spray axis region is smaller than that of the spray periphery at all pressure conditions. The distribution tendencies of the size of these droplets fairly resemble the pattern of inversely bell-shaped, which is consistent with characteristics of the pressure-swirl nozzle [37]. The reason is that the liquid discharging from the nozzle orifice forms the hollow-cone spray shape and it is concentrated at the spray periphery

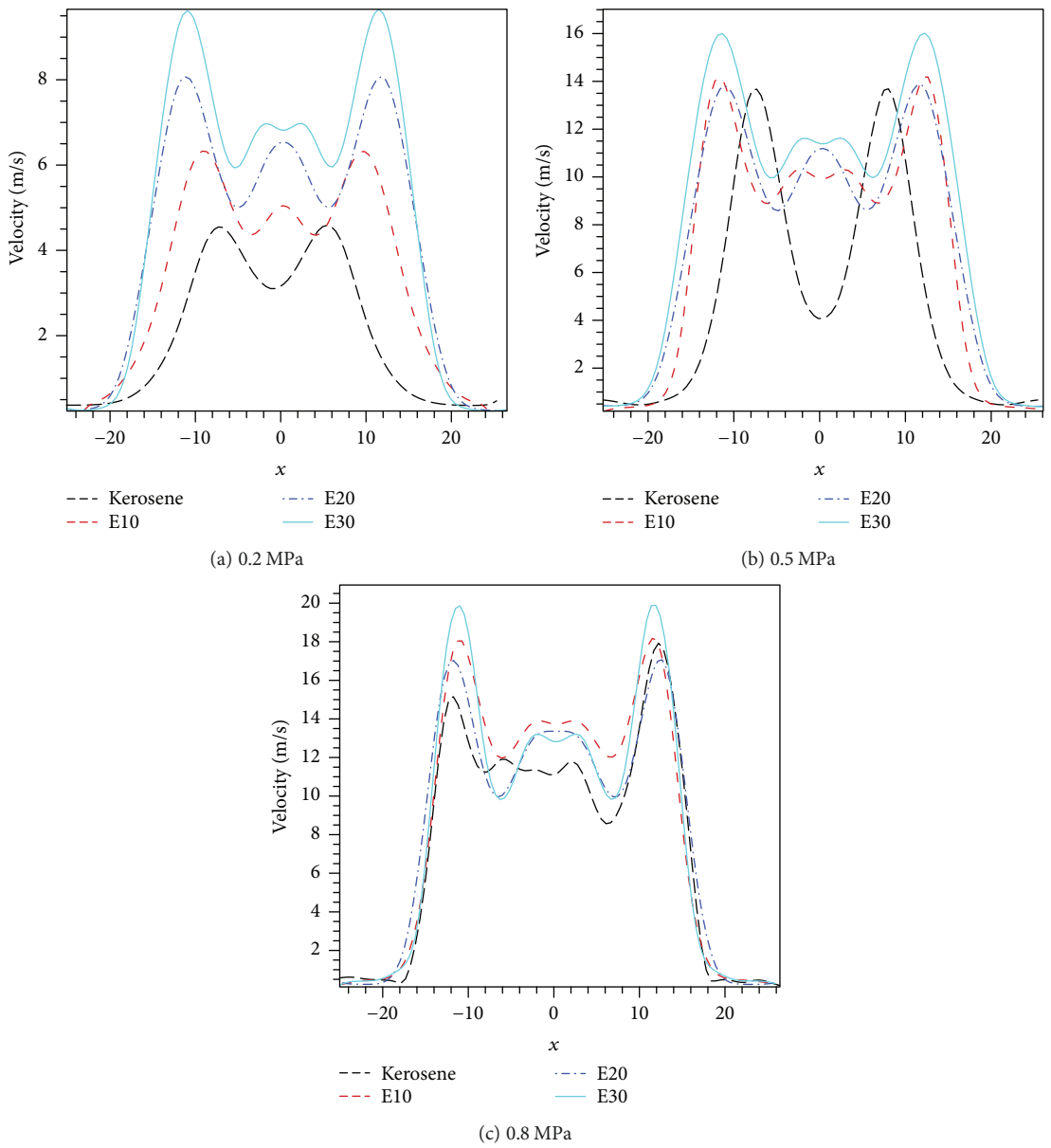

Figure 16: The velocity profiles of blended fuel at $y = -20$ mm under pressures of 0.2, 0.5, and 0.8 MPa.

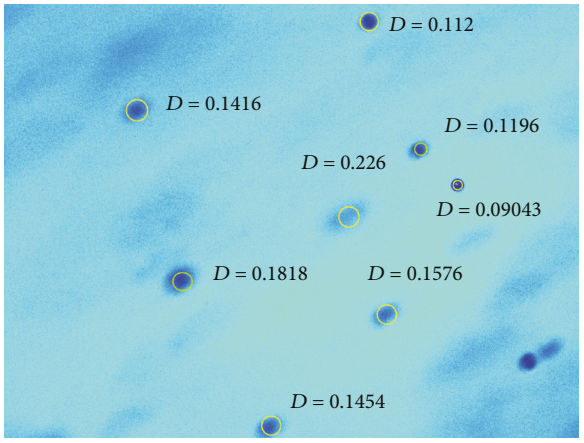

Figure 17: Droplet diameters processed by DaVis software.

under the sufficient centrifugal force. In addition, the SMD of droplets decreases as the ethanol concentration and the injection pressure increase. This is because the fuels rapidly disintegrate developing along the motion trajectory due to the lower viscosity. Meanwhile, it stands to reason that smaller spray droplets are produced with sufficient swirl intensity at higher injection pressure.

Compared with kerosene, the SMDs of E10, E20, and E30 decrease on average by 13.9% (21.0% or 2.5%), 31.3% (23.0% or 5.0%), and 33% (24.8% or 7.3%) at the condition of 0.1 MPa (0.5 MPa or 0.8 MPa), respectively. The SMDs of droplets change significantly at low injection pressure while it does not vary prominently under high injection pressure. The SMD variation with radial distance is less distinct at higher pressure, which has little influence on SMD for the blended fuels. This is because the mass flux is proportional to the injection pressure and then mass flux growth is

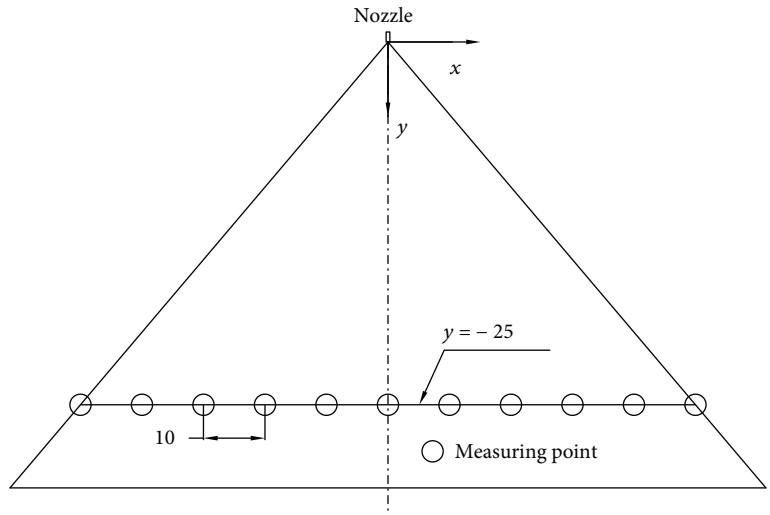

Figure 18: The measuring point position of the spray body.

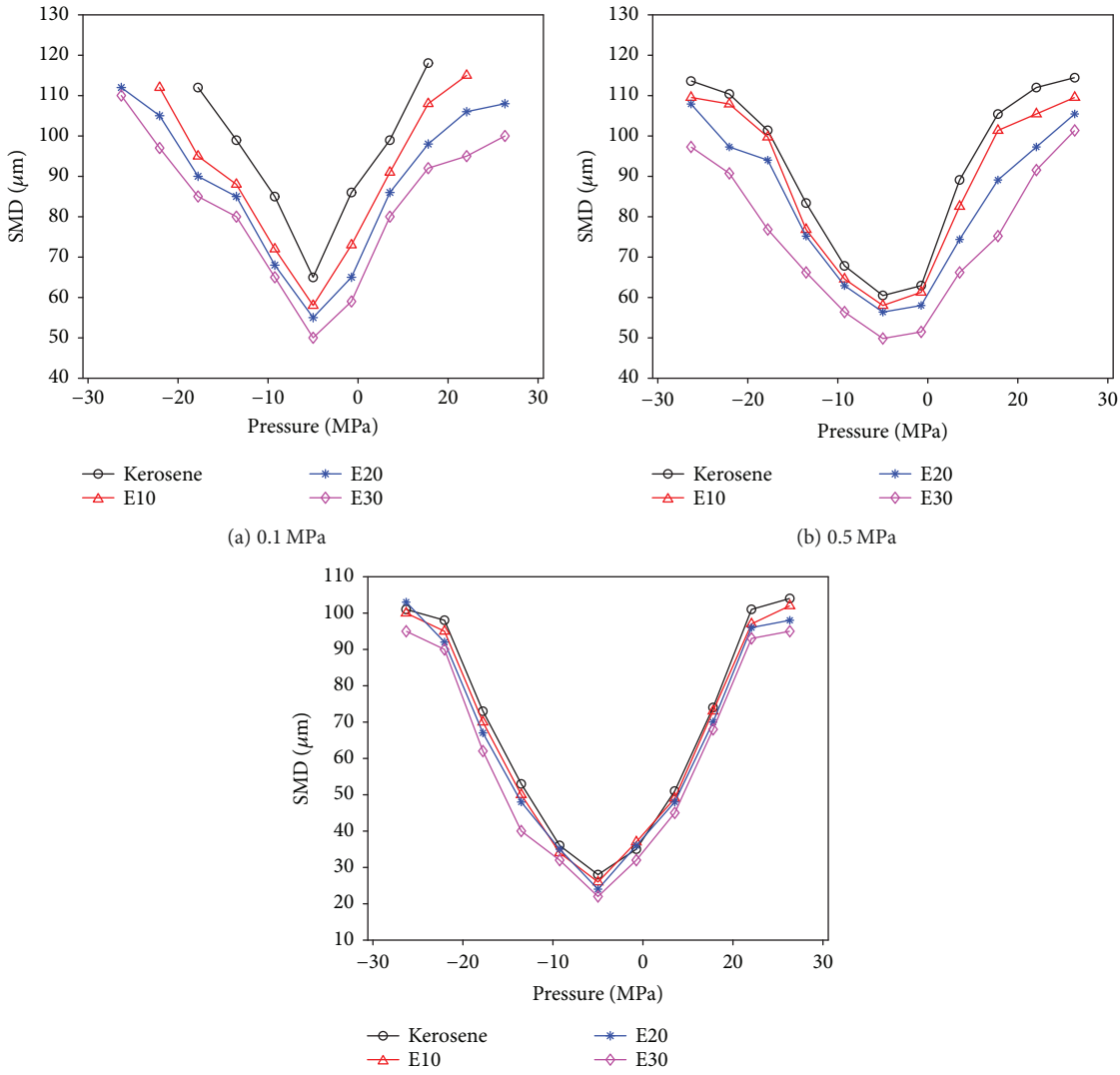

Figure 19: The SMD of blended fuels at $y = -25$ mm under 0.1, 0.5, and 0.8 MPa.

beyond the atomization ability of this pressure-swirl nozzle. At 0.8 MPa, the mass flow rate is almost the same regardless of the fluid viscosity. According to the relationship between SMD, Q, and μ (SMD $\propto \mu^{0.25}Q^{0.25}$) presented by Lefebvre [22, 38], the SMD is not affected significantly by the viscosity. Comparison of SMD values in the radial direction of the four blended fuels expresses that the adding of ethanol into kerosene can produce fine spray at low pressure.

4. Conclusion

In the present work, an experimental study has been carried out to study the spray characteristic of blended fuel discharging from a pressure-swirl nozzle. The results show that the adding of ethanol into the kerosene can promote the spray quality. In summary, the conclusions and outlook are listed as follows.

The spray cone angle increases with the injection pressure. When the pressure is increased to 0.8 MPa, the spray cone angle almost attains the maximum value (nozzle design value) regardless of the ethanol concentration. At the same injection pressure, higher ethanol concentration results in bigger spray cone angle. Compared with kerosene, the spray cone angles of E10, E20, and E30 increase on average by 2.58%, 5.15%, and 7.87%, respectively. The empirical formula proposed by Lefebvre is proved to be suitable for the spray cone angle of kerosene-ethanol blends.

The discharge coefficient and the breakup length decrease with both injection pressure and ethanol concentration. Besides, with further increase in the injection pressure, the discharge coefficients of different blends decrease to a steady value, where it almost remains stable. Compared with kerosene, the discharge coefficients of E10, E20, and E30 decrease on average by 4.3%, 7.4%, and 10.1%, respectively. The discharge coefficients predicted by Jones' previous formula are larger than experimental results due to the different swirler angles.

A new method is introduced to measure the breakup length. It is found out that the breakup length decreases with the injection pressure and ethanol concentration. Compared with kerosene, the breakup lengths of E10, E20, and E30 decrease on average by 10.6%, 20.3%, and 43.1%, respectively. The corrected relation to breakup length relation agrees well with the experimental results.

The droplet velocity magnitude profile and drop size are significantly affected by the injection pressure. The experimental results show that these spray characteristics are greatly affected at the low injection pressure, while they are slightly influenced under high injection pressure. The pressure-swirl nozzle produces the solid-cone spray changing into a hollow-cone spray with the increase in ethanol concentration and injection pressure. At high injection pressure (exceeds 0.8 MPa), the spray velocity distribution and drop size are almost the same regardless of the ethanol concentration in blended fuel. The SMD of the blended fuel decreases as ethanol concentration increases at $y = -25$ mm under the same condition. Therefore, the spray performance shows good atomization at low injection pressure when ethanol is added into kerosene, while ethanol concentration has little impact on the spray characteristics at high pressure.

The present work only experimentally studied spray characteristics. The liquid will eventually burns in the combustion chamber. Therefore, the combustion characteristics will be considered for different ethanol ratios of the blends in future work.

Data Availability

The data used to support the findings of this study are available from the corresponding author upon request.

Conflicts of Interest

The authors declare that they have no conflicts of interest.

Acknowledgments

The work was jointly sponsored by the National Natural Science Foundation of China (NSFC) under Grant No. 51776031 and the key project of the National Natural Science Foundation of Liaoning Province of China under Grant No. 20170540182.

References

[1] A. H. Lefebvre and J. Ortman, "Fuel distributions from pressure-swirl atomizers," *Journal of Propulsion and Power*, vol. 1, no. 1, pp. 11–15, 1985.

[2] V. Dorfner, J. Domnick, F. Durst, and R. Kohler, "Viscosity and surface tension effects in pressure swirl atomization," *Atomization and Sprays*, vol. 5, no. 3, pp. 261–285, 1995.

[3] I. Chung and C. Presser, "Fluid property effects on sheet disintegration of a simplex pressure-swirl atomizer," *Journal of Propulsion and Power*, vol. 17, no. 1, pp. 212–216, 2001.

[4] C. Dopazo and J. Ballester, "Discharge coefficient and spray angle measurements for small pressure-swirl nozzles," *Atomization and Sprays*, vol. 4, no. 3, pp. 351–367, 1994.

[5] E. Wimmer and G. Brenn, "Viscous flow through the swirl chamber of a pressure-swirl atomizer," *International Journal of Multiphase Flow*, vol. 53, no. 1, pp. 100–113, 2013.

[6] A. K. Azad, S. M. A. Uddin, and M. M. Alam, "Experimental study of DI diesel engine performance using biodiesel blends with kerosene," *International Journal of Energy and Environment*, vol. 4, no. 2, pp. 265–278, 2013.

[7] C. J. Mendez, R. N. Parthasarathy, and S. R. Gollahalli, "Performance and emission characteristics of butanol/Jet A blends in a gas turbine engine," *Applied Energy*, vol. 118, no. 1, pp. 135–140, 2014.

[8] P. G. Aleiferis, J. Serras-Pereira, A. Augoye, T. J. Davies, R. F. Cracknell, and D. Richardson, "Effect of fuel temperature on in-nozzle cavitation and spray formation of liquid hydrocarbons and alcohols from a real-size optical injector for direct-injection spark-ignition engines," *International Journal of Heat and Mass Transfer*, vol. 53, no. 21-22, pp. 4588–4606, 2010.

[9] T. N. C. Anand, A. M. Mohan, and R. V. Ravikrishna, "Spray characterization of gasoline-ethanol blends from a multi-hole port fuel injector," *Fuel*, vol. 102, no. 6, pp. 613–623, 2012.

[10] Y. Fan, N. Hashimoto, H. Nishida, and Y. Ozawa, "Spray characterization of an air-assist pressure-swirl atomizer injecting high-viscosity Jatropha oils," *Fuel*, vol. 121, no. 2, pp. 271–283, 2014.

[11] L. A. B. Cortez, F. E. B. Nigro, L. A. H. Nogueira et al., "Perspectives for sustainable aviation biofuels in Brazil," *International Journal of Aerospace Engineering*, vol. 2015, Article ID 264898, 12 pages, 2015.

[12] A. K. Agarwal and V. H. Chaudhury, "Spray characteristics of biodiesel/blends in a high pressure constant volume spray chamber," *Experimental Thermal and Fluid Science*, vol. 42, no. 42, pp. 212–218, 2012.

[13] H. Bayraktar, "Experimental and theoretical investigation of using gasoline–ethanol blends in spark-ignition engines," *Renewable Energy*, vol. 30, no. 11, pp. 1733–1747, 2005.

[14] H. L. Maclean and L. B. Lave, "Evaluating automobile fuel/propulsion system technologies," *Progress in Energy and Combustion Science*, vol. 29, no. 1, pp. 1–69, 2003.

[15] S. K. Chen, A. H. Lefebvre, and J. Rollbuhler, "Factors influencing the effective spray cone angle of pressure-swirl atomizers," *Journal of Engineering for Gas Turbines and Power*, vol. 114, no. 1, pp. 97–103, 1992.

[16] J. Chen, J. Li, and L. Yuan, "Effects of inlet pressure on ignition of spray combustion," *International Journal of Aerospace Engineering*, vol. 2018, Article ID 3847264, 13 pages, 2018.

[17] B. S. Park, H. Y. Kim, and S. S. Yoon, "Transitional instability of a pressure-swirl atomizer due to air-core eruption at low temperature," *Atomization and Sprays*, vol. 17, no. 6, pp. 551–568, 2006.

[18] A. Kushari and P. Barman, "Primary liquid breakup in a pressure-swirl atomizer," *International Journal of Fluid Mechanics Research*, vol. 35, no. 4, pp. 354–364, 2008.

[19] S. Lee, W. Kim, and W. Yoon, "Spray formation by a swirl spray jet in low speed cross-flow," *Journal of Mechanical Science and Technology*, vol. 24, no. 2, pp. 559–568, 2010.

[20] L. Song, T. Liu, W. Fu, and Q. Lin, "Experimental study on spray characteristics of ethanol-aviation kerosene blended fuel with a high-pressure common rail injection system," *Journal of the Energy Institute*, vol. 91, no. 2, pp. 203–213, 2016.

[21] A. Sinha, R. S. Prakash, A. M. Mohan, and R. V. Ravikrishna, "Experimental studies on evaporation of fuel droplets under forced convection using spray in crossflow methodology," *Fuel*, vol. 164, no. 37, pp. 374–385, 2016.

[22] A. H. Lefebvre, *Atomization and Sprays*, Hemisphere Pub. Corp, 1988.

[23] M. S. F. M. Rashid, A. H. A. Hamid, O. C. Sheng, and Z. A. Ghaffar, "Effect of inlet slot number on the spray cone angle and discharge coefficient of swirl atomizer," *Procedia Engineering*, vol. 41, no. 2, pp. 1781–1786, 2012.

[24] A. Datta and S. K. Som, "Numerical prediction of air core diameter, coefficient of discharge and spray cone angle of a swirl spray pressure nozzle," *International Journal of Heat and Fluid Flow*, vol. 21, no. 4, pp. 412–419, 2000.

[25] S. Yao, J. Zhang, and T. Fang, "Effect of viscosities on structure and instability of sprays from a swirl atomizer," *Experimental Thermal and Fluid Science*, vol. 39, no. 5, pp. 158–166, 2012.

[26] D. Kim, J. H. Im, H. Koh, and Y. Yoon, "Effect of ambient gas density on spray characteristics of swirling liquid sheets," *Journal of Propulsion and Power*, vol. 23, no. 3, pp. 603–611, 2007.

[27] Z. Lan, D. Zhu, W. Tian, G. Su, and S. Qiu, "Experimental study on spray characteristics of pressure-swirl nozzles in pressurizer," *Annals of Nuclear Energy*, vol. 63, no. 1, pp. 215–227, 2014.

[28] M. R. Soltani, K. Ghorbanian, M. Ashjaee, and M. R. Morad, "Spray characteristics of a liquid–liquid coaxial swirl atomizer at different mass flow rates," *Aerospace Science and Technology*, vol. 9, no. 7, pp. 592–604, 2005.

[29] L. Bayvel and Z. Orzechowski, *Liquid Atomization*, 1993.

[30] G. N. Laryea and S. Y. No, "Spray angle and breakup length of charge-injected electrostatic pressure-swirl nozzle," *Journal of Electrostatics*, vol. 60, no. 1, pp. 37–47, 2004.

[31] Z. Han, S. Parrish, P. V. Farrell, and R. D. Reitz, "Modeling atomization processes of pressure-swirl hollow-cone fuel sprays," *Atomization and Sprays*, vol. 7, no. 6, pp. 663–684, 1997.

[32] N. K. Rizk and A. H. Lefebvre, "Internal flow characteristics of simplex swirl atomizers," *Journal of Propulsion and Power*, vol. 1, no. 3, pp. 193–199, 1985.

[33] N. Dombrowski and P. C. Hooper, "The effect of ambient density on drop formation in sprays," *Chemical Engineering Science*, vol. 17, no. 4, pp. 291–305, 1962.

[34] D. Kim, P. Han, J. H. Im, Y. Yoon, and V. G. Bazarov, "Effect of recess on the spray characteristics of liquid-liquid swirl coaxial injectors," *Journal of Propulsion and Power*, vol. 23, no. 6, pp. 1194–1203, 2012.

[35] Q. F. Fu, L. J. Yang, Y. Y. Qu, and B. Gu, "Linear stability analysis of a conical liquid sheet," *Journal of Propulsion and Power*, vol. 26, no. 5, pp. 955–968, 2014.

[36] L. Durdina, J. Jedelsky, and M. Jicha, "Investigation and comparison of spray characteristics of pressure-swirl atomizers for a small-sized aircraft turbine engine," *International Journal of Heat and Mass Transfer*, vol. 78, no. 7, pp. 892–900, 2014.

[37] L. Durdina, J. Jedelsky, and M. Jicha, "Experimental investigation on spray characteristics of pressure-swirl atomizers for a small-sized jet engine," in *12th Triennial International Conference on Liquid Atomization and Spray Systems*, pp. 1–8, Heidelberg, Germany, September 2012.

[38] A. H. Lefebvre and X. F. Wang, "Mean drop sizes from pressure-swirl nozzles," *Journal of Propulsion and Power*, vol. 3, no. 1, pp. 11–18, 1987.